Contents list available at IJRED website

International Journal of Renewable Energy Development

Journal homepage: https://ijred.undip.ac.id

Research Article

# Multifunctional Bangka kaolin for zeolite 3A pellet synthesis and its application in ethanol dehydration

Maria Ulfah[1*], Pasymi Pasymi[1], Amelia Amir[1], Ulung Muhammad Sutopo[1], Burmawi[2], Melia Laniwati Gunawan[3], I.G.B.N. Makertihartha[3]

[1]*Department of Chemical Engineering, Faculty of Industrial Technology, Universitas Bung Hatta, Padang, 25146, Indonesia*

[2]*Department of Mechanical Engineering, Faculty of Industrial Technology, Universitas Bung Hatta, Padang, 25146, Indonesia*

[3]*Department of Chemical Engineering, Faculty of Industrial Technology, Institut Teknologi Bandung, Bandung, 40132, Indonesia*

**Abstract**. The development of cost-effective, highly efficient adsorbents for bioethanol dehydration is crucial to advancing sustainable biofuel integration, including the upcoming E10 fuel-blending mandates in Indonesia. This study evaluates the multifunctional capability of locally sourced Bangka kaolin as both a structural precursor and an active binder for the synthesis of binder-converted Zeolite 3A pellets, specifically tailored for ethanol-water azeotrope separation. The fabrication procedure followed a comprehensive two-stage method, commencing with the thermal calcination of raw kaolin at 600°C and 750°C to generate reactive metakaolin. Subsequently, a hydrothermal synthesis strategy was employed using different alkalinity settings, governed by $H_2O/Na_2O$ molar ratios of 40, 43, and 45, corresponding to NaOH concentrations of 2.88 M, 2.67 M, and 2.55 M, respectively. This solution-gel matrix was homogenized with synthesized Zeolite Na-A powder, extruded into pellets, and subjected to an in-situ hydrothermal crystallization phase to transform the amorphous binder into a crystalline Zeolite A framework. Final structural modification was performed via successive liquid-phase potassium-ion exchanges using 21 wt.% and 11 wt.% chloride potassium solutions to shrink the effective pore opening to approximately 3A. Structural and compositional assessments via X-ray diffraction (XRD) and X-ray fluorescence (XRF) confirmed the successful formation of Zeolite A frameworks with no residual sodium oxide (0.00% $Na_2O$), achieving significant potassium loading (30.15–34.58 wt.% $K_2O$) and moderate relative crystallinities ranging from 55% to 74%. Textural diagnostics from $N_2$ physisorption demonstrated that the synthesized pellets exhibit an IUPAC Type IV isotherm coupled with a Type H3 hysteresis loop, indicating a hierarchically organized pore structure with crucial secondary mesopores. Performance evaluation during dynamic ethanol-water separation confirmed that the synthesized Zeolite 3A pellets exhibit an enhanced water adsorption capacity of up to 27.97 wt.% for the ZKA-750-45 sample, yielding fuel-grade bioethanol with a peak purity of 99.7 wt.%.

**Keywords:** Bangka kaolin, calcination, metakaolin, palletizations, zeolite 3Å

@ The author(s). Published by CBIORE. This is an open access article under the CC BY-SA license (https://creativecommons.org/licenses/by-sa/4.0/).

Received: 12th March 2026; Revised: 17th May 2026; Accepted: 28th May 2026; Available online: xxxx 2026

## 1. Introduction

B35 was implemented in Indonesia beginning in early February 2023, involving the blending of 35% biodiesel with diesel fuel. This program aims to achieve several objectives: reduce carbon emissions, decrease dependence on imported fossil fuels, support the palm oil industry, and create new economic opportunities. The Indonesian government is also focusing on developing other biofuels, including bioethanol. The Indonesian government plans to introduce E10 bioethanol by 2025, a fuel blend consisting of 10% bioethanol and 90% gasoline. The bioethanol used in these fuel blends must have a minimum purity of 99.5 wt.%. Fuel-grade ethanol, also known as gasohol, meets this requirement with a purity level above 99.5 wt.%, making it suitable for fuel mixtures. However, conventional distillation is limited to producing a maximum ethanol concentration of approximately 95 wt.%, as the formation of the ethanol-water azeotrope restricts the process. A promising method for producing fuel-grade ethanol is the adsorption process, which utilizes zeolite A as the adsorbent (Simo *et al.*, 2009; Abdeen *et al.*, 2011; Shukla *et al.*, 2019).

Zeolite A, also known as Zeolite Linde Type A (Zeolite LTA), was the first synthetic zeolite to be commercially produced in 1956. Its primary building block is a sodalite framework composed of four rings that form a three-dimensional (3D) network, as shown in Figure 1 (Nakano & Nozue, 2007). Including alkali cations is necessary to balance the valence difference between aluminum (+3) and silica (+4). These cations can be exchanged for others using ion-exchange techniques. Depending on the exchangeable cation-potassium, sodium, or calcium ion, it is also called Zeolite 3A, 4A, or 5A, respectively (Breck *et al.*, 1956). Zeolite 3Å is widely recognized as an effective material for separating ethanol and water. It has an average pore opening of 3Å. Water molecules, with a diameter of 2.6 Å, can readily enter the pore structure of 3Å adsorbents, whereas larger ethanol molecules (5.2 Å) are excluded. Additionally, water remains trapped in the 3Å sodalite cage of zeolite because it is more polar than ethanol (Abdeen *et al.*, 2011).

Kaolin can serve as a raw material for zeolite synthesis because its main components are $Al_2O_3$ and $SiO_2$. The availability of kaolin in Indonesia, especially in Bangka Belitung,

* Corresponding author:
Email: mariaulfah@bunghatta.ac.id (M Ulfah)

https://doi.org/10.61435/ijred.2026.62522
ISSN: 2252-4940/© 2026.The Author(s). Published by CBIORE

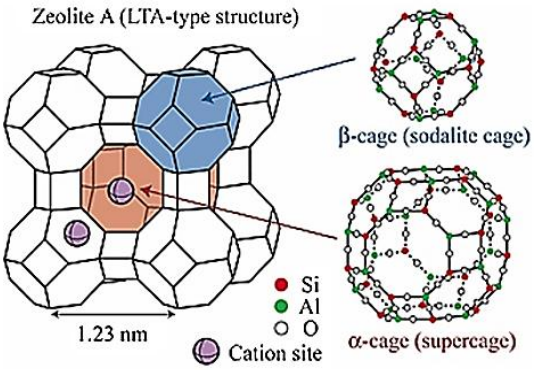


**Fig. 1** Schematic representation of LTA zeolite (Nakano and Nozue, 2007)

is abundant, totalling 376.687.532 tons. The kaolin deposits in Bangka are generally white, fine-textured, soft, low in iron and titanium, and relatively high in silica and alumina (Nurhidayati *et al*., 2020). Many research papers have been reported on the synthesis of zeolite 4A from kaolin (Gougazeh & Buhl, 2014; Maia *et al.,* 2015; Lim *et al.,* 2021; Eluwa *et al*., 2024). However, previous research has mainly focused on identifying the conditions for producing zeolite A in fine powder form. In commercial-scale adsorber column applications, the zeolite extruded form is preferred because it experiences less fluid-pressure loss than the powder form. The zeolite extruded can be made using five components: a silica source, an alumina source, alkali, water, and a binder. Kaolin can serve as a source of alumina and silica, which are the main materials for synthesizing zeolite A powder and are also used as binders. However, the kaolin binder must be converted to zeolite to improve its water-adsorption capacity. Research has been conducted on the production of zeolite A pellets using Bangka kaolin as a binder, with water glass and sodium aluminate serving as the silica and alumina sources, respectively. The study found that Bangka kaolin, when used as a binder, can be transformed into zeolite (Ulfah *et al*., 2020).

The production of zeolite A from kaolin involves a two-step procedure: initially, kaolin undergoes calcination, resulting in the formation of metakaolin; followed by hydrothermal treatment of metakaolin with an aqueous NaOH solution to produce zeolite 4A. The effective production of Zeolite Na-A requires a comprehensive understanding of the factors influencing the formation of highly reactive metakaolin. Furthermore, the yield and structural quality of the synthesized Zeolite 4A are influenced by intrinsic differences in the properties of clays from various geographical locations (Maia *et al.,* 2014). Crucially, the optimal calcination temperature for forming reactive amorphous metakaolin depends on the degree of crystallinity and the overall mineralogical composition of the kaolin (Kirdeciler & Akata, 2020; Kovo *et al*., 2025; Pasabeyoglu et al., 2023).

Rocha *et al*., (1991) showed that metakaolin obtained from Cornish kaolinite and calcined at 700°C exhibited increased reactivity toward the formation of zeolite A. Chandrasekhar (1996) determined that the ideal calcination temperature for China clay from Kerala, India, was 900°C for one hour. This procedure produced a highly reactive metakaolin capable of forming detergent-grade zeolite 4A, noted for its excellent crystallinity and brightness. Pasabeyoglu *et al.* (2023) reported that Zeolite 4A synthesized from Turkish kaolin was successfully produced, with crystallinity exceeding 90% across all products. This high crystallinity was achieved by preparing metakaolin from kaolin calcined within the optimal temperature range of 740$^0$C to 860◦C. Ultimately, Abdullahi *et al.,* (2017) established three categories for the metakaolinisation reaction temperature: a low range of 400–500°C, a moderate range of 600–800°C, and a high range of 800–900°C. The specific kaolin calcination temperatures adopted in this study, namely 600 and 750°C, were positioned within the moderate temperature range.

The alkalinity of the synthesis solution, along with the calcination temperature of kaolin, is an essential factor that greatly affects the properties of zeolite 4A. Gougazeh and Buhl (2014) produced zeolite A from natural kaolin sourced from Jordan, which had undergone calcination at 650$^0$C. Their research found that zeolite A was the main product when the concentration of NaOH varied between 1.50 and 3.50 M. Maia *et al.* (2015) synthesized zeolite A using kaolin obtained from two different regions in Brazil, Capim (KC) and Jari (KJ), while investigating Na/Al ratios ranging from 1.36 to 1.64. They found that a high-purity Na-A zeolite with an enhanced degree of structural order was achieved at a Na/Al ratio of 1.64 for both kaolin types, KC and KJ. Aliyu *et al.,* (2020) investigated the influence of the activating solution on the synthesis of zeolite A prepared from kaolin from Grahamstown, South Africa. They reported that a 1.0 M NaOH solution failed to produce any measurable amount of zeolite. Upon increasing the concentration to 2.0 M, the initial crystalline phase appeared, exhibiting a cubic, rounded zeolite A morphology. When the concentration was further raised to 3.0 M NaOH, well-defined cubic crystals of zeolite A were produced. Ultimately, at a 4.0 M NaOH concentration, the resulting product exhibited significantly enhanced growth of cubic zeolite A crystals, although traces of unreacted amorphous aluminosilicate remained visible.

This research aimed to examine Bangka kaolin's multiple roles as a source of silica, alumina, and binder for synthesizing 3A zeolite pellets. Additionally, the study evaluated the performance of the developed 3A zeolite as an adsorbent for the ethanol dehydration process. This study also investigated the effects of kaolin calcination temperature and $H_2O/Na_2O$ molar ratios 40, 43, and 45 (corresponding to 2.88 M, 2.67 M, and 2.55 M, respectively) during the synthesis of zeolite A powder on its water adsorption performance from ethanol-water mixtures.

## 2. Materials and methods

### *2.1 Materials*

The research utilized kaolin, a natural mineral sourced from Bangka Province, Indonesia; potassium chloride obtained from Merck; technical-grade sodium hydroxide (NaOH) pellets with 98% purity; 96% technical-grade ethanol; commercial zeolite X; and distilled water.

### *2.2 Synthesis Zeolite Na-A Powder*

The synthesis of zeolite Na-A powder from kaolin involves two stages: (1) converting kaolin to produce metakaolin under thermal conditions, and (2) reacting metakaolin with aqueous NaOH in an HDPE bottle without shaking. This research produced metakaolin by calcining kaolin at 600°C (MK600) and 750°C (MK750) at a heating rate of 5 K/min in a muffle furnace with a temperature programmer.

The effect of alkalinity on zeolite A was examined by reacting each metakaolin sample (MK600 and MK750) with NaOH solutions at $H_2O/Na_2O$ molar ratios of 40, 43, and 45 (2.88 M, 2.67 M, and 2.55 M, respectively). The calcined metakaolin was combined with an aqueous sodium hydroxide (NaOH) solution. The mixture was then stirred for 15 minutes at room temperature to ensure homogeneity. The gels from the

**Table 1**
Nomenclature of the synthesized zeolite Na-A powder

| Starting material | Ratio mol $H_2O/Na_2O$ (Molar, M) | Product |
|---|---|---|
| MK600 | 40 (2.88) | ZNaA-600-40 |
| MK600 | 43 (2.67) | ZNaA-600-43 |
| MK600 | 45 (2.55) | ZNaA-600-45 |
| MK750 | 40 (2.88) | ZNaA-750-40 |
| MK750 | 43 (2.67) | ZNaA-750-43 |
| MK750 | 45 (2.55) | ZNaA-750-45 |

**Table 2**
Nomenclature of the synthesized zeolite KA pellet

| Binders | Zeolite Na-A powder | Product |
|---|---|---|
| MK600 | ZNaA-600-40 | ZKA-600-40 |
| MK600 | ZNaA-600-43 | ZKA-600-43 |
| MK600 | ZNaA-600-45 | ZKA-600-45 |
| MK750 | ZNaA-750-40 | ZKA-750-40 |
| MK750 | ZNaA-750-43 | ZKA-750-43 |
| MK750 | ZNaA-750-45 | ZKA-750-45 |

reacted mixtures were aged at approximately 20°C for 114 hours. After aging, the metakaolin gels were heated at 100°C for 47 hours to promote crystallization. The resulting zeolite was then washed with distilled water until the wash water reached pH 9, and then dried at 100°C for 24 hours. The symbol for the produced zeolite Na-A corresponds to the calcination temperature of the kaolin and aqueous NaOH concentrations, as shown in Table 1.

*2.3 Synthesis Zeolite 3Å Pellet*

Three grams of metakaolin and four grams of zeolite Na-A powder are mixed and stirred for 15 minutes. The mixture is subsequently mixed with the NaOH solution and stirred until a consistent paste forms. This paste was extruded and left at room temperature for 24 hours in a high-density polyethylene container filled with NaOH solution, then crystallized at 100°C for 24 hours to convert metakaolin into zeolite. The resulting samples are washed with distilled water until the pH reaches 9. Zeolite Na-A (4A) can be transformed into zeolite 3A by exchanging $Na^+$ cations in Na-A zeolite with $K^+$ cations. In this study, cation exchange was performed twice using different concentrations of potassium chloride solution at each stage. In the first and second stages, solutions with potassium chloride concentrations of 21 wt.% and 11 wt.% were used, respectively. In this process, 4 mL of a potassium chloride solution containing exchangeable potassium was mixed with 1 g of zeolite Na-A. The exchange was carried out in a shaker at 60°C for 2 hours. The produced zeolite 3A (ZKA) was washed to remove residual sodium, then dried and activated. The resulting zeolite 3A (ZKA) designation corresponds to the metakaolin calcination temperature and the zeolite Na-A type, as shown in Table 2.

*2.4 Characterization*

Elemental composition samples were analyzed using a Spectrometer EDXRF instrument (PANalytical Epsilon 4, B.V., Almelo, The Netherlands). The crystalline phases of the materials were identified from X-ray powder diffraction (XRD) patterns using Cu Kα radiation at 40 kV and 30 mA. Data were collected over a range of 5 to 80° 2θ at a scan speed of 0.04° 2θ/s with an X'Pert Pro (PANalytical B.V., Almelo, The Netherlands). The degree of crystallinity (%) was quantified using Origin Pro software, following Sazali and Harun (2022).

$$Crystallinity = \frac{Area\ of\ crystalline\ peaks}{Area\ of\ all\ peak\ (crystalline+amorphous)} \quad (1)$$

Morphological observations and measurements were conducted using a field emission scanning electron microscope (FE-SEM; Quattro S from Thermo-Fisher Scientific, United States). The $N_2$ physisorption experiment was performed using a Quantachrome instrument (Anton Paar Quanta Tec Inc., Boynton Beach, USA). The external surface area and micropore volume were determined using the **t**-plot method based on the Halsey thickness equation, as described by Lowell *et al.*, (2004).

*2.5 Performance Test of Adsorbent Zeolite 3A Pellets*

The performance test equipment for the developed zeolite 3A adsorbent is illustrated in Figure 2. The distillation flask contained 1000 ml of an ethanol-water mixture, and the adsorbent column held 20 g of zeolite pellets. Ethanol with 95% purity is heated in a heating mantle to 78°C. The ethanol-water vapor mixture passes through the zeolite A pellet. The water is

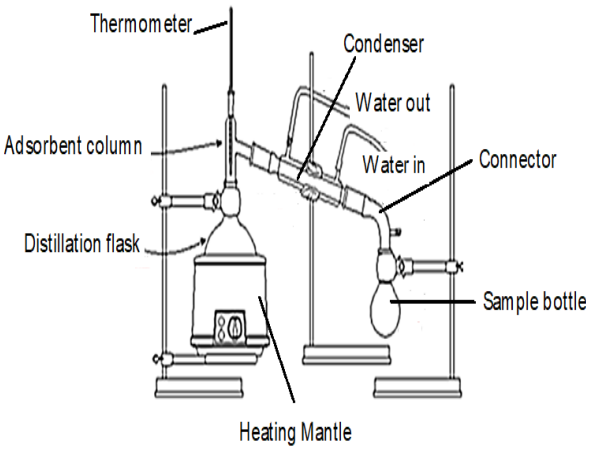


**Fig 2.** The setup for the adsorption process

trapped in the pores of the zeolite pellet, while the ethanol vapor enters the condenser, where it condenses from vapor to liquid. The distillate obtained from the distillation process is collected in a sample bottle to a volume of up to 270 ml for concentration measurement using an alcoholmeter. Sampling was conducted until the ethanol concentration reached a steady state.

## 3. Result and Discussion

Figure 3 shows the physical form of the zeolites produced by varying the kaolin calcination temperature (600 and 750°C) and the concentration of the NaOH solution ($H_2O/Na_2O$ molar ratios of 40, 43, and 45 or 2.88 M, 2.67 M, and 2.55, respectively) used for preparing a metakaolin-NaOH sol-gel mixture. The syntheses were conducted using only Bangka kaolin, sodium oxide, and distilled water. The chemical composition of Bangka kaolin is detailed in Table 3.

Zeolite A intended for industrial applications is typically manufactured in pellet/granule/bead forms through hydrothermal crystallization of a carefully formulated solution containing silicon, aluminium, sodium, and a binding agent. In this research, Bangka kaolin is utilized as a source of silica and alumina and as a binding agent.

### *3.1 Kaolin*

Pure kaolin ($Al_2O_3{\cdot}2SiO_2{\cdot}2H_2O$) has an ideal molar ratio of silicon to aluminium (Si/Al) of 1. However, the Si/Al ratio of Bangka kaolin is greater than 1 (see Table 3), indicating the presence of excess silica ($SiO_2$) in the sample. This excess silica usually results from mineral impurities, with quartz ($SiO_2$) being the most common impurity (Hartati *et al.,* 2020). Figure 4a shows that Bangka kaolin is composed of a primary crystalline kaolinite ($Al_2Si_2O_5(OH)_4$) phase, characterized by peaks at 2θ = 12.5° and 25°. The presence of quartz is also confirmed by the X-ray diffraction (XRD) profile shown in Fig. 4a, which displays characteristic peaks at 2θ = 20.87° and 26.6° (Moore & Reynolds, 1997). Similarly, Pasabeyoglu *et al.,* (2025), Król and Rożek (2018), Sazali and Harun (2022), and Yin *et al.,* (2024) reported that the main components of kaolin from Turkey, Poland, Malaysia, and China, respectively, consist of kaolinite and quartz.

Certain minor oxides in kaolin typically undergo minimal alteration during calcination. For instance, the $Fe_2O_3$ concentration decreased from 2.352% to 2.203% in MK600, and further to 2.012% in MK750. Kirdeciler and Akata (2020) noted that iron content does not significantly affect the zeolite product. The $TiO_2$ concentration rose from 0.301% to 0.378% in MK600 and peaked at 0.575% in MK750. Crucially, the high reactivity of metakaolin typically promotes the formation of a highly crystalline zeolite phase, which is likely to predominate in the final product (Hart *et al.,* 2025). Furthermore, the activity of metakaolin is influenced by the temperature at which the kaolin is calcined (Król & Rożek, 2018; Pasabeyoglu *et al.,* 2023; Kovo *et al.,* 2025).

### *3.2 Metakaolin*

The chemical composition of MK600 and MK750 is shown in Table 3. As detailed in Table 3 (XRF analysis), following calcination, the weight percentage of the primary oxide, $Al_2O_3$, increased, while that of $SiO_2$ decreased. In MK600, the $Al_2O_3$ proportion increased from 34.297% in the unprocessed kaolin to 36.543%, whereas the $SiO_2$ proportion decreased from 56.643% to 54.870%. A comparable trend was noted for the sample calcined at 750 °C. The meta-kaolinization process reduces the Si/Al molar ratio, which declines from 1.40 in raw kaolin to 1.28 in MK600 and further to 1.20 in MK750. This reduction signifies that the metakaolin produced is alumina-rich. A Si/Al ratio < 2 is particularly advantageous for synthesizing zeolites with low Si/Al ratios, such as zeolite A (LTA), which has an approximate Si/Al ratio of 1, and zeolite X


**Fig. 3** Synthetic zeolite: (a) ZKA-600-40, (b) ZKA-600-43, (c) ZKA-600-45, (d) ZKA-750-40, (e) ZKA-750-43, (f) ZKA-750-45, (g) Commercial Zeolite X

**Table 3**
Chemical analysis of kaolin and metakaolin

| | Kaolin | MK600 | MK750 |
|---|---|---|---|
| $Al_2O_3$ | 34.297 | 36.543 | 37.908 |
| $SiO_2$ | 56.643 | 54.870 | 53.508 |
| $P_2O_5$ | 3.332 | 3.144 | 3.192 |
| $K_2O$ | 2.021 | 1.86 | 1.719 |
| CaO | 0.724 | 0.634 | 0.634 |
| $TiO_2$ | 0.301 | 0.378 | 0.575 |
| $V_2O_5$ | 0.003 | 0.002 | 0.006 |
| MnO | 0.017 | 0.014 | 0.012 |
| $Fe_2O_3$ | 2.352 | 2.203 | 2.012 |
| ZnO | 0.007 | 0.008 | 0.011 |
| Si/ Al | 1.40 | 1.28 | 1.20 |

(FAU), which spans a Si/Al ratio from 1 to 1.5. This is due to the favourable stoichiometric conditions required to create these frameworks. The high reactivity of metakaolin with a low Si/Al ratio is crucial for facilitating rapid dissolution and subsequent crystallization (Lekha & Nambiar, 2018).

The X-ray diffraction (XRD) patterns of metakaolin (MK600 and MK750) are shown in Fig. 4. Following calcination, the kaolinite peaks significantly diminish, and the material develops a broad amorphous metakaolin signature represented by a halo peaking between 15° and 36° (2θ). This change confirms that thermal activation causes the collapse of the kaolinite structure and the formation of a highly reactive, amorphous metakaolin. This amorphous phase is crucial because it is highly soluble in alkaline solutions, providing the silica and alumina precursors necessary for zeolite growth (El Bojaddayni *et al.,* 2023). In both MK600 and MK750, the peaks from admixed impurities and the quartz peak remain clearly visible. This persistence of quartz is consistent with reports from Pasabeyoglu *et al.,* (2023) and Kirdeciler and Akata (2020). According to Pasabeyoglu *et al.,* (2023), the quartz peaks remained consistent in intensity as the calcination temperature increased, even when kaolin was heated to 980°C. Moreover, kaolin containing more than 5% quartz cannot be effectively removed through the meta-kaolinization process (Kirdeciler & Akata, 2020).

### *3.2 Synthesized Zeolite*

#### *3.2.1 X-ray diffraction analysis*

The XRD patterns of the six products synthesized are

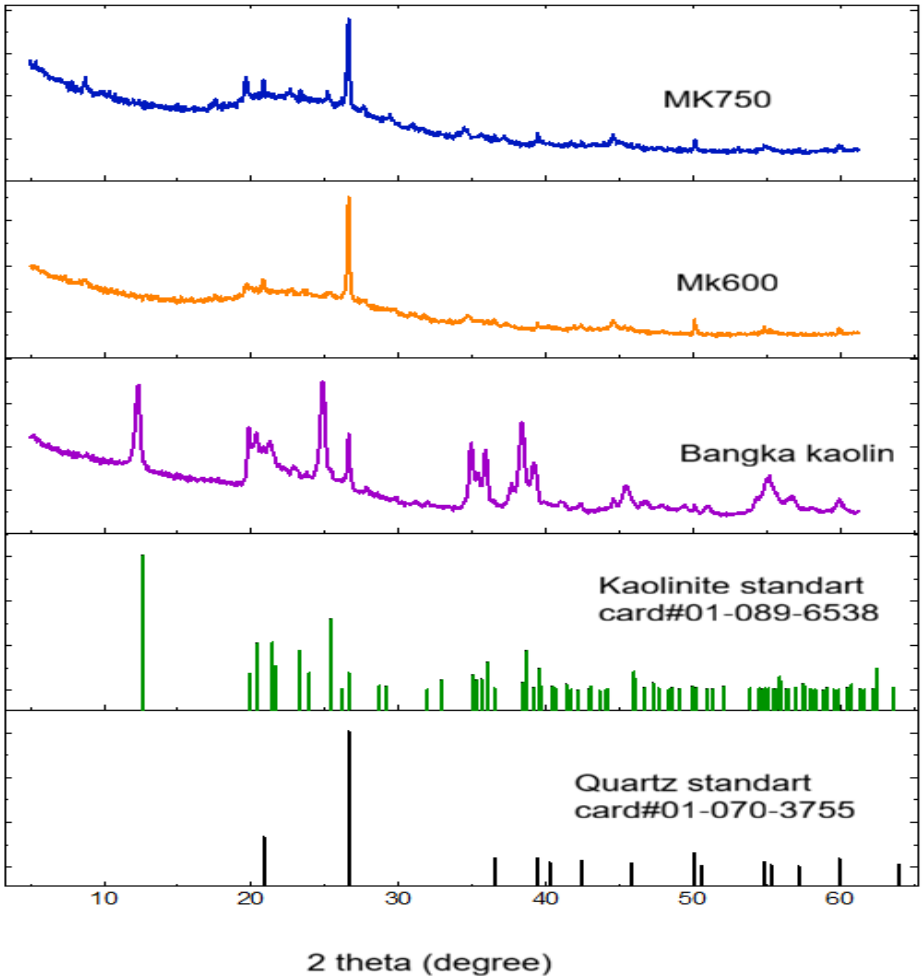


**Fig. 4.** XRD patterns of raw kaolin and metakaolin

shown in Fig. 5. The diffractograms for all zeolite sample display nearly identical patterns. They are characterized by a series of sharp peaks at approximately 2θ (degree) = 7.1, 10.1, 12.4,16.2, 21.6, 24, 26, 27.2, 30, 30.9, 32.6, 34.2, and 42.5. Compared with simulated XRD powder patterns of zeolites (IZA), this pattern is typical of Zeolite A (Linde Type A, LTA framework)(Treacy & Higgins, 2001). The fact that most of the peaks are attributable to zeolite A and appear sharp with minimal background noise indicates a moderate level of purity and crystallinity for all zeolite A samples. This research is a direct extension of earlier studies that demonstrated the effectiveness of local kaolin as a suitable precursor for synthesizing zeolite A (Aliyu *et al.,* 2020; Sazali & Harun, 2022; Sinchangreed *et al.*, 2025). However, those prior investigations were solely focused on producing zeolite in powder form. The major contribution of the current work lies in the successful utilization of calcined Bangka kaolin (i.e., metakaolin) as a binder during the pelletization phase. This application advances the use of locally sourced materials from simple synthesis to the enhanced production of functional, shaped zeolite products.

The pelletization process involved mixing zeolite A powder with metakaolin dissolved in a NaOH solution, maintaining a 4:3 weight ratio between zeolite A powder and metakaolin. The XRD patterns (see Fig. 5) provided strong evidence that a considerable amount of the metakaolin binder was converted in situ to the zeolite A phase during processing, thereby increasing the overall zeolite A content in the final pellets. While the attainment of such a moderate level of binder conversion is commendable, diffractogram analysis continually reveals a minor peak at a 2θ angle of approximately 26.5°. This particular peak, indicative of the quartz ($SiO_2$) phase, indicates the presence of a residual crystalline impurity in the Bangka kaolin source material, albeit at a significantly lower concentration. The ability to produce zeolite A pellets and to achieve effective binder conversion has significant implications for industrial applications that demand solid, shaped materials with optimal mechanical strength and exceptional ion-exchange and molecular sieving properties (Gleichmann *et al.,* 2016).

The next step is to investigate the effect of activation temperature on zeolite A formation. From the XRD diffractogram displayed in Figure 5, the samples activated at 600 and 750°C successfully formed the intended zeolite A structure, although amorphous material was also identified. Compared with ZKA600, a significant sodalite phase was detected in the ZKA750 zeolite diffractogram, as indicated by the diffraction peak at 2θ = 13.84 °. These results have also been reported by Filho *et al.*, (2015) and Król and Rożek (2018). Higher activation temperatures facilitate the synthesis of hydroxy-sodalite, a material with a structural configuration beneficial for sorption processes (Król & Rożek, 2018).

The effect of the kaolin calcination temperature on the formation of zeolite A is described in the following description. The synthesis of zeolite A via alkali activation was accomplished by optimally calcining metakaolin at 700°C (Król & Rożek, 2018). Zhou *et al.,* (2014) stated that metakaolin derived from kaolin calcined at 730°C is significantly activated and ideal for producing zeolite A. Pasabeyoglu *et al.*, (2023) demonstrated that calcination temperatures between 740 and 860°C effectively balance amorphous material with the nucleation of spinel to achieve optimal zeolite A, although the details can differ depending on the source of the clay and the conditions of the synthesis. Azhar *et al.,* (2024) showed that if metakaolin is not fully synthesized at a slightly lower temperature of 600°C, it results in the creation of a solid zeolite structure known as

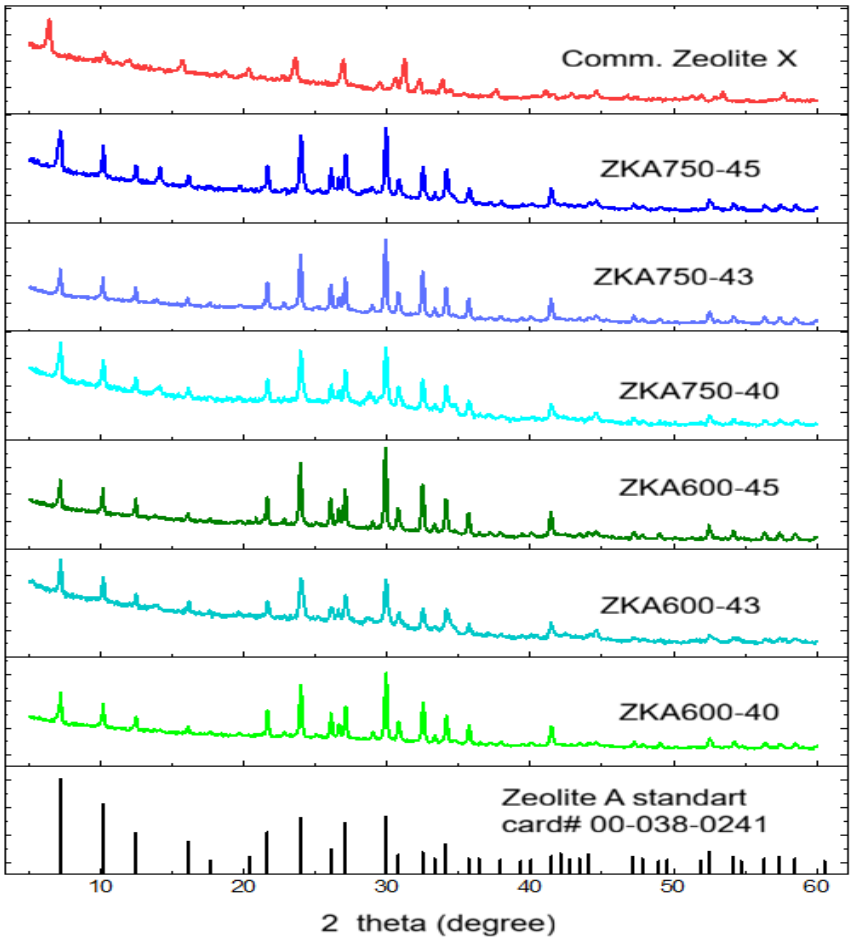


**Fig. 5** XRD Patterns of Synthesized and Commercial Zeolite

sodalite. Conversely, slightly increasing the calcination temperature to 650°C leads to more complete metakaolin formation, thereby facilitating the full development of the zeolite A phase. Filho *et al.,* (2015) documented the relative crystallinities of zeolite A obtained from samples calcined at 550, 600, 700, and 800°C, which were 47%, 52%, 52%, and 45%, respectively. A decrease in octahedral aluminium is associated with rising temperatures, indicating that calcining kaolin between 600 and 700°C is essential. The hydrothermal production of zeolite A from kaolin as the raw material is still under study due to differing opinions on the conditions required to obtain metakaolin. There are varied perspectives on the activation temperature of kaolin, which depend on the origin of the raw material.

Another factor that influences the formation of zeolite A is the NaOH concentration. In the study we conducted, NaOH solution was used under three conditions: first, during the synthesis of powdered zeolite; second, to create a paste mixture of powdered zeolite and metakaolin; and finally, during the crystallization phase of the extrusion process. As evidenced by the XRD diffractogram (Figure 5), the intended zeolite A structure was successfully synthesized via alkali activation at $H_2O/Na_2O$ molar ratios of 40, 43, and 45. The sodalite phase (SOD), a competing phase in zeolite A synthesis, is also detected in ZKA750-45, exhibiting a greater peak intensity at 2θ=13.84∘ than that observed in ZKA750-40. For ZKA-600, the sodalite phase was not detected, even when the NaOH concentration was increased to 45%. For comparison, Sinchangreed *et al.*, (2025) reported that the optimal conditions for producing zeolite A were achieved using NaOH concentrations of 3 and 4 M, with the mixture heated to 200°C for 24 hours. However, the zeolite A pattern was not detected at NaOH concentrations of 1 and 2 M. Sazali and Harun (2022) synthesized Na-A zeolite using an NaOH concentration 0.5, 1, 2 and 3 M. Their results indicated that the crystallinity of Na-A zeolite rises from 62.83% to 86.8% as the NaOH molarity increases from 0.5 M to 1 M; however, when the NaOH molarity is further raised to 1 M and 2 M, it does not increase (recording 80.77% and 67.78%, respectively). The optimal alkalinity increased the dissolution rate of Si and Al ions, thereby aiding in the development of appropriate Na-A zeolite crystal nuclei. The presence of favorable nuclei significantly affects the crystallization of Na-A zeolite (Lim *et al.,* 2021). Higher alkalinity is known to increase impurity levels and promote the decomposition of the zeolite structure, thereby reducing its relative crystallinity (Liu *et al.,* 2013; Gougazeh & Buhl, 2014). Figure 6 shows the combined effect of calcination temperature and NaOH solution concentration on the crystallinity of the synthesized zeolite A pellets, which was determined using Origin Pro software according to Equation (1). At a calcination temperature of 600◦C, the crystallinity decreased from 72.25% to 64.38% as the $H_2O/Na_2O$ molar ratio

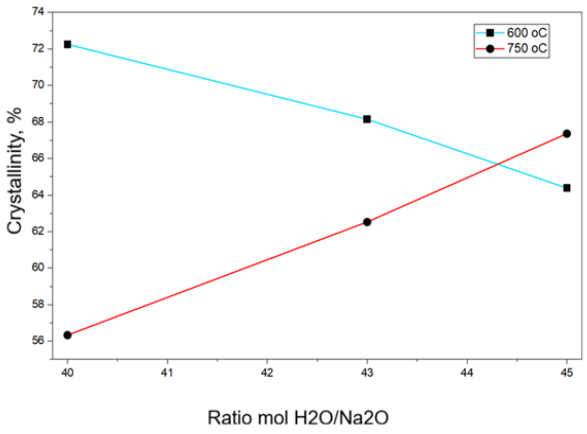


**Fig. 6** Crystallinities (%) of Synthesized Zeolite A Pellet

increased from 40 to 45. However, the opposite trend was observed at a kaolin calcination temperature of 750°C: the crystallinity increased from 56.33% to 67.36% as the NaOH concentration increased. The findings suggest that high-quality zeolite A pellets can be effectively produced through the synergistic effects of calcination temperatures (600°C and 750°C) and NaOH solution concentration. In research conducted by Król and Rożek (2018), Na-A zeolite was synthesized from kaolin precursors (ME600, ME700, and ME800) using various NaOH molarities (3.0–9.0 M). Their findings highlighted critical process conditions: at a synthesis temperature of 70°C (24h), zeolite A was formed only from the ME600 and ME700 precursors and required a high NaOH concentration of 9.0 M. The phase was notably absent when ME800 was used at 70°C, regardless of concentration. However, the activation of ME800 (with 9 M NaOH) did successfully yield zeolite A when the synthesis temperature was increased to 90°C. Increasing the calcination temperature often leads to excessive dehydroxylation and the premature formation of mullite (or other crystalline/non-reactive amorphous phases). These high-temperature phases are thermodynamically stable but exhibit lower chemical reactivity when subjected to the alkaline (NaOH) solution. This reduced reactivity hinders the complete dissolution-reprecipitation process essential for crystallization, thereby decreasing the overall crystallinity of zeolite A (Yin *et al.,* 2021).

### *3.2.2 X-ray Fluorescence (XRF) analysis*

The comprehensive chemical compositions of the 6 synthesized products were determined using XRF analyses and are presented in Table 4. The XRF data revealed a notable

**Table 4**
Chemical analysis of zeolite ZKA and Commercial zeolite X

| Component, % | ZKA600 ratio mol $H_2O/Na_2O$ ( M ) | | | ZKA750 ratio mol $H_2O/Na_2O$ ( M ) | | | Commercial zeolite X |
|---|---|---|---|---|---|---|---|
| | 40 (2.88) | 43 (2.67) | 45 (2.55) | 40 (2.88) | 43 (2.67) | 45 (2.55) | |
| $Na_2O$ | 0.00 | 0.00 | 0.00 | 0.00 | 0.00 | 0.00 | 4.459 |
| $Al_2O_3$ | 9.174 | 9.227 | 9.126 | 9.908 | 9.703 | 9.842 | 11.32 |
| $SiO_2$ | 53.661 | 53.631 | 52.912 | 56.100 | 55.292 | 56.693 | 80.113 |
| $P_2O_5$ | 0.014 | 0.014 | 0.014 | 0.016 | 0.015 | 0.015 | 0.022 |
| $K_2O$ | 33.920 | 33.736 | 34.582 | 30.718 | 31.733 | 30.154 | 0.63 |
| CaO | 0.274 | 0.286 | 0.265 | 0.277 | 0.290 | 0.261 | 0.296 |
| $TiO_2$ | 0.308 | 0.314 | 0.303 | 0.428 | 0.398 | 0.427 | 0.044 |
| $Fe_2O_3$ | 1.314 | 1.353 | 1.299 | 1.388 | 1.336 | 1.356 | 0.432 |
| Si/ Al | 4.96 | 4.93 | 4.92 | 4.80 | 4.83 | 4.89 | 6.00 |

**Table 5**
The textural properties of synthesized zeolite ZKA600-45, ZKA750-45 and commercial zeolite X.

| Samples | BET surface area, ($m^2/g$) [a] | Total pore volume, ($cm^3/g$) | t-plot method | | | |
|---|---|---|---|---|---|---|
| | | | t-plot Equation | $S_{micro}$ ($m^2/g$ | $S_{ext}$ ($m^2/g$ | $V_{micro}$ ($cm^3/g$) |
| ZKA600-45 | 5.129 | 0.0181 | y = 0.923x - 2.062 | 12.2 | 14.28 | nil |
| ZKA750-45 | 6.912 | 0.0182 | y = 0.548x - 0.884 | 7.6 | 8.48 | nil |
| Commercial zeolite X. | 445.716 | 0.2433 | y = 1.496x + 3.978 | 33. 6 | 23.14 | 0.0061 |

[a] Multipoint BET

compositional characteristic: sodium oxide ($Na_2O$) was not detected in any of the six samples (0.00%). Concurrently, a significant concentration of potassium oxide ($K_2O$) was observed, with values ranging from 30.154% to 34.582%. This result is consistent with the production method for zeolite 3A, which involves the exchange of $Na^+$ ions (from Zeolite 4A) for $K^+$ ions.

Silica ($SiO_2$) and alumina ($Al_2O_3$) are the fundamental constituents of the zeolite framework. The alumina content remained relatively consistent, ranging from 9.126 wt.% to 9.908 wt.% across all samples. The silica content was substantially higher, ranging from 52.912% to 56.693%. Generally, the samples calcined at a higher temperature (ZKA750) exhibited slightly higher percentages of $SiO_2$ and $Al_2O_3$ than those calcined at ZKA600. The measured Si/Al ratio for all samples ranged from 4.80 to 4.96. This ratio is significantly higher than the theoretical Si/Al ratio for standard zeolite A, which is ideally 1 (or $SiO_2/Al_2O_3 \approx 2$). A Si/Al ratio approaching 5 suggests that the resulting material is not phase-pure zeolite A. This is also consistent with the calculated crystallinity of ZKA, which ranged from 55% to 74%. A high Si/Al ratio indicates that the material is silica-rich. A probable cause is the presence of unreacted silica ($SiO_2$) from the raw materials, which was concurrently detected by the XRF analysis. This phenomenon is common when the reactant ratios are non-stoichiometric for zeolite A formation.

*3.2.3 $N_2$ physisorption Analysis*

The nitrogen adsorption-desorption isotherms of the synthesized zeolite and commercial zeolite are illustrated in Figure 7, while the corresponding textural properties are summarized in Table 5. According to the International Union of Pure and Applied Chemistry (IUPAC) classification, both the ZKA600-45 and ZKA750-45 samples exhibit Type IV isotherms. This isotherm type is characterized by a hysteresis loop (the region where the adsorption and desorption branches do not

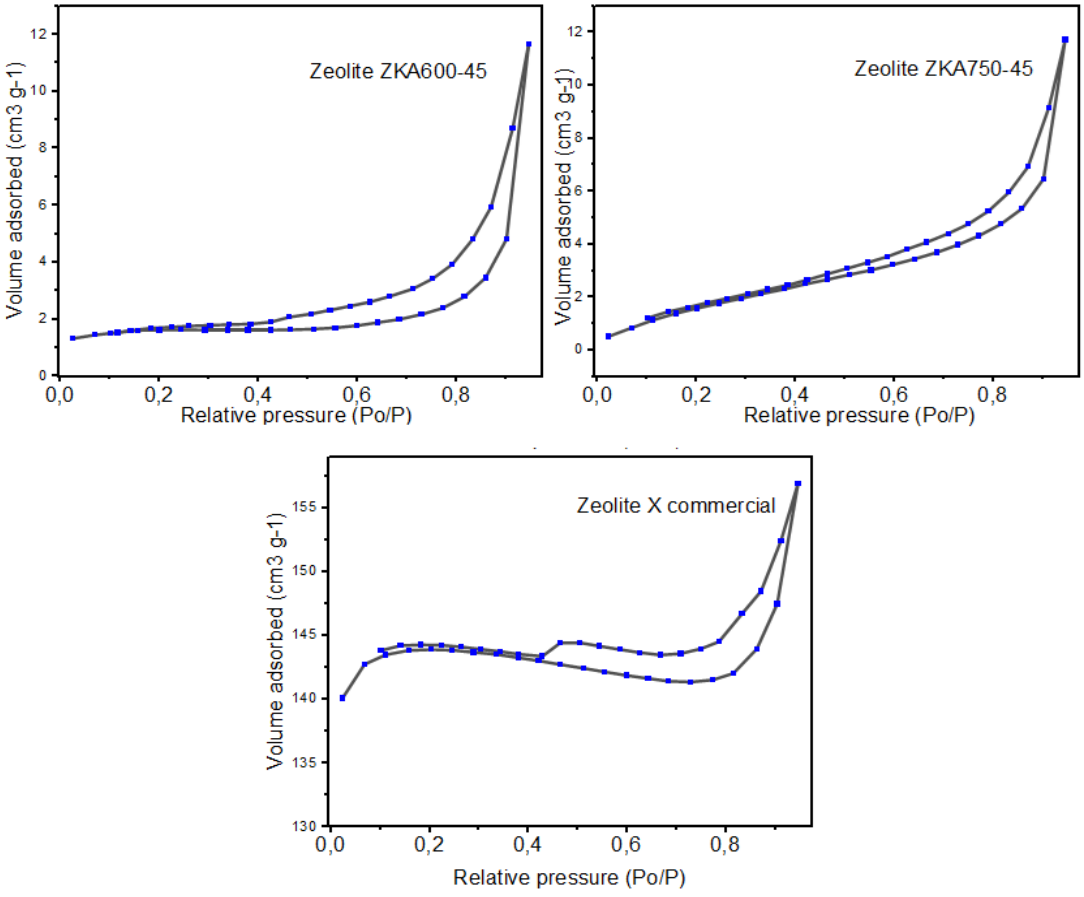


**Fig 7**. The $N_2$ adsorption-desorption isotherm of synthesized zeolite ZKA600-45, ZKA750-45, and zeolite X commercial

coincide) at a relatively high range of relative pressure (P/Po), approximately 0.4 to 1.0. A Type IV isotherm is indicative of mesoporous materials (defined as having pore diameters between 2 and 50 nanometers). The shape of the hysteresis loop in both plots resembles Type H3, which is characterized by the absence of a distinct saturation plateau at high P/Po values. This type of loop is commonly associated with particle aggregates that form slit-shaped pores (Thommes *et al.,* 2015).

The comparative t-plot analysis reveals a significant influence of the treatment temperature on the textural evolution of the synthesized zeolites. Sample Z600-45 exhibits a higher external surface area ($S_{ext}$ = 14.28 $m^2/g$) compared to Z750-45 ($S_{ext}$ = 8.48 $m^2/g$). This reduction in surface area at higher temperatures suggests a partial sintering effect or structural collapse of the secondary mesopore walls as the temperature increases from 600°C to 750°C. In addition, ZKA600-45 has a higher K2O content than ZKA750-45 (34.582% vs. 30.154%; Table 4), which is consistent with its larger surface area.

*3.2.4 SEM Analysis*

Figure 8 shows the SEM morphology of ZKA600-45, ZKA750-45, and commercial zeolite X. From Figure 8 (a and b), it can be observed that the morphology of ZKA600-45 is similar to that of the ZKA750-45 sample. The particles of both zeolites exhibit a distinct cubic crystal shape. This cubic crystal morphology is highly characteristic of zeolite A (LTA) (Zhao *et al*., 2014; Lim *et al*., 2021). The Scanning Electron Microscopy (SEM) results corroborate the X-Ray Diffraction (XRD) results, indicating that the synthesis products, ZKA600-45 and ZKA750-45, have successfully formed the zeolite A phase. The morphology of the commercial zeolite X particles (Figure 8c) appears predominantly larger and possesses an octahedral shape. The octahedral morphology is a typical feature of Zeolite X or Y (Yao *et al*., 2018).

*3.3 Water Adsorption Equilibrium Experiment*

A comparative study of water adsorption on synthesized zeolite and commercial zeolite X is shown in Table 6. Table 6 presents the ranking of water adsorption effectiveness as follows: ZKA-750-45 exhibited the highest water adsorption capacity (27.97 wt.%) and yielded the highest ethanol purity in sample 1 (99.7 wt.%). The performance of ZKA-600-45 was marginally inferior to that of ZKA-750-45, adsorbing 27.3 %wt. Commercial zeolite X demonstrated the lowest water adsorption capacity within this group (26.3 wt.%). Based on these performance data, both synthesized zeolites (ZKA) outperformed commercial zeolite X in ethanol dehydration applications. According to the commercial specification provided by the manufacturer, the commercial SNOWPEAK 3A molecular sieve pellets exhibit a static $H_2O$ adsorption capacity exceeding 21.5% (≥21.5%) during ethanol dehydration. This potassium-sodium aluminosilicate features a chemical formula of $0.4K_2O.0.6\ Na_2O.\ Al_2O_3.\ 2SiO_2.\ 4.5H_2O$ with a molar ratio $SiO_2$: $Al_2O_3$ of approximately 2 (Si/Al ≈ 1), indicating that its primary structural framework comprises $K_2O$, $Na_2O$, $Al_2O_3$, $SiO_2$, and $H_2O$ (https://www.snowpeakzeolite.com/product-item/molecular-sieve-3a/). According to the EDXRF data presented in Table 4, the synthesized zeolite contains no $Na_2O$. The $Na^+$ cation exchange during the synthesis of the developed zeolite was performed twice using KCl solutions at concentrations of 21 wt.% and 11 wt.%, respectively. This successive treatment likely induced the complete replacement of $Na^+$ cations (initially as $Na_2O$) by $K^+$ cations ($K_2O$). Paranuk *et al*., (2018) highlighted that the batch composition in the crystallization process, the precursors used, and the exchange techniques are crucial factors influencing the selective adsorption capacity of zeolites. The structural windows of the zeolite framework, where $Na^+$ or $K^+$ cations are situated, act as steric barriers that govern the penetration of water molecules.

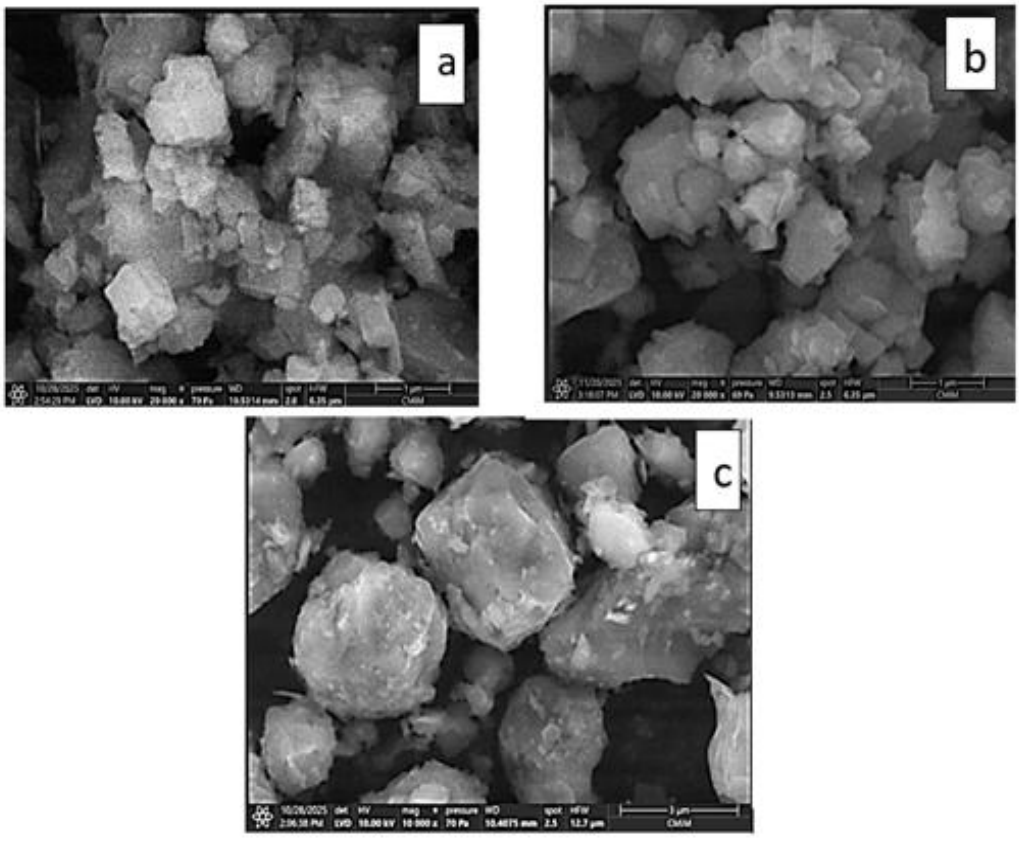


**Fig 8**. Scanning electron microscopy (SEM) morphology: (a) ZKA600-45, (b) ZKA750-45, and commercial zeolite X.

**Table 6**
Performance Evaluation of Synthesized and Commercial Zeolites for Water Adsorption from 95% Ethanol-Water Mixtures

| Sample | Ethanol purity (%) | | | Water adsorbed, % |
|---|---|---|---|---|
| | sample 1 | sample 2 | sample 3 | |
| ZKA-600-40 | 99.3 | 99 | 97 | 25.6 |
| ZKA-600-43 | 99.5 | 99 | 97.5 | 25.33 |
| ZKA-600-45 | 99.6 | 99 | 97 | 27.28 |
| ZKA-750-40 | 99.5 | 99.2 | 96 | 27.3 |
| ZKA-750-43 | 99.7 | 99.5 | 97 | 27.81 |
| ZKA-750-45 | 99.7 | 99.5 | 97.3 | 27.97 |
| Zeolite X commercial | 99 | 99 | 96 | 26.3 |

Therefore, modifying the composition, abundance, and distribution sites of these alkali cations can systematically alter the effective pore opening, resulting in tunable water adsorption capacities (Ramírez *et al*., 2021). In hydrophilic frameworks like LTA- and FAU-type zeolites, water adsorption is dictated by a combination of available pore volume, framework-oxygen binding, and interaction with compensating cations within the solvation layer. These mechanisms are fundamentally driven by electrostatic attractions arising from the polarized nature of both the water molecules and the host zeolite structure (Tahraoui *et al*., 2020). Water vapor molecules are bonded with the cation type $K^+$ much more strongly than with the $Na^+$ cations (Al Ezzi & Ma, 2017).

Data trends in Table 6 indicate that increasing the binder calcination temperature from 600°C to 750°C consistently enhances the water adsorption capacity. The superior performance of ZKA-750-45 is closely linked to the reactivity of the metakaolin precursor used. According to Mejía de Gutiérrez *et al*. (2008), calcination temperatures in the range of 700–800°C are optimal for maximizing the chemical reactivity of metakaolin. This is due to the formation of unstable, penta-coordinated aluminium ($Al^V$) species during the de-hydroxylation of kaolinite. This transition state is highly reactive and essential for rapid, high-crystallinity zeolite synthesis, as it facilitates efficient dissolution of silica and alumina sources during the hydrothermal process.

Morphologically, SEM analysis reveals that ZKA-750-45 possesses significantly cleaner crystal surfaces. In contrast, ZKA-600-45 exhibits remnants of unreacted binder that may obstruct diffusion pathways. This is further supported by the higher crystallinity of ZKA-750-45 than that of ZKA-650-45 (Figure 6). The plate-like particle aggregates observed in ZKA-750-45 are highly consistent with the Type H3 hysteresis loop identified in the nitrogen isotherms, signifying an open, slit-shaped pore architecture. This structure effectively minimizes internal mass transfer resistance and eliminates the internal diffusion limitations often encountered in purely microporous materials (Pérez-Botella *et al*., 2022).

The efficiency of adsorption-based separation processes depends directly on the molecular transport rate inside zeolite pores. Controlling this adsorption rate and molecular motion can be achieved by tailoring diffusion pathways via the manipulation of crystal or pore sizes. Recent advances in synthesis methods have shifted toward hierarchical zeolites—materials synthesized by aggregating nanocrystals to incorporate secondary meso- or macro-porosity. This hierarchical structure successfully addresses the mass transfer limitations and restricted accessibility characteristic of conventional zeolites. Due to their multimodal pore-size distribution (including micro-, meso-, and/or macropores), hierarchical zeolites significantly reduce diffusion distances and accelerate mass transfer. These features are important for catalysis, separation processes, and adsorption (Sachse *et al*., 2017). Consequently, investigations into hierarchical zeolites have expanded substantially over the last one decade (Chen *et al*., 2012; Verboekend *et al*., 2016; Ramírez *et al*., 2021).

## 4. Conclusion

In summary, this study successfully demonstrated the multifunctional capability of locally sourced Bangka kaolin as both a silica-alumina precursor and a reactive binding agent for fabricating binder-converted Zeolite 3A pellets. The two-stage synthesis protocol—comprising thermal calcination within a moderate temperature window (600–750°C) and subsequent alkali hydrothermal activation—effectively induced the *in-situ* transformation of the metakaolin binder into the crystalline Zeolite Na-A phase. X-ray diffraction (XRD) and X-ray fluorescence (XRF) analyses confirmed the successful synthesis of structurally stable Zeolite A configurations. The resulting materials exhibited moderate purity, with relative crystallinities ranging from 55% to 74% and a substantial $K_2O$ loading of 30–34 wt.%.

Furthermore, textural evaluation via $N_2$ physisorption revealed a distinct Type IV isotherm, indicating the formation of an advantageous pore structure with secondary mesopores, which is highly critical for intensifying mass transport. Performance evaluations in ethanol dehydration revealed that the developed Zeolite 3A pellets exhibit excellent molecular sieving and robust water adsorption, enabling the successful removal of water from ethanol-water azeotropes, yielding high-purity, fuel-grade bioethanol. These findings offer a cost-effective, sustainable, and scalable strategy to advance the utilization of abundant natural clay minerals from simple powder-form synthesis toward high-performance, shaped industrial adsorbents tailored for advanced biofuel purification.

**Acknowledgements.** The authors gratefully acknowledge the Ministry of Higher Education, Science, and Technology of Indonesia for financial support, and Universitas Bung Hatta (Padang, Indonesia) for providing access to their laboratory facilities and equipment in support of this research.

**Author contributions.** Conceptualization: MU; methodology: MU, ML, IGBN M; formal analysis and investigation: ML, IGBN M; writing—

original draft preparation: MU; writing—review and editing: P, B, AA, and UMS; funding acquisition: MU; resources: AA, and UMS; supervision: MU. All authors read and approved the final manuscript.

**Funding** The authors express their gratitude to the Fundamental Research Grant Scheme (FRGS), Ministry of Higher Education, Science and Technology, Indonesia, Grant 131/C3/DT.05.00/PL/2025.

**Compliance with ethical standards**
Conflict of interest the authors declare that they have no conflict of interest.

## References

Abdeen, F. R. H., Mel, M., Al-Khatib, M., & Azmi, A. S. (2011). Dehydration of ethanol on zeolite-based media using adsorption process. *Proceedings of the 3rd CUTSE International Conference*, Sarawak, Malaysia.

Abdullahi, T., Harun, Z., & Othman, M. H. D. (2017). A review on sustainable synthesis of zeolite from kaolinite resources via hydrothermal process. *Advanced Powder Technology*, *28*(8), 1827–1840. https://doi.org/10.1016/j.apt.2017.04.028

Aliyu, U. M., Rathilal, S., Mustapha, S. I., & Isa, Y. M. (2020). Hydrothermal synthesis and characterization of zeolite A from Grahamstown South Africa kaolin. *Proceedings of the 18th South Africa International Conference on Agricultural, Chemical, Biological & Environmental Sciences (ACBES-20)*, Johannesburg, South Africa.

Al Ezzi, A. and Ma, H., 2017. Equilibrium adsorption isotherm mechanism of water vapor on zeolites 3A, 4A, X, and Y. In *Proceedings of the ASME 2017 International Mechanical Engineering Congress and Exposition. Volume 8: Energy*. Tampa, Florida, USA, November 3–9, 2017. V008T10A101. ASME. https://doi.org/10.1115/IMECE2017-72601.

Azhar, F. H., Harun, Z., Hanafi, W. N. F. A., Sazali, N., Hussin, R., Kamdi, Z., Ainuddin, R., Yunos, M. Z., & Ismail, A. (2024). Zeolite synthesis from natural kaolin: The effect of metakaolin heating and transformation. *Emerging Advances in Integrated Technology*, *5*(1), 75–81. https://doi.org/10.30880/emait.2023.05.01.010

Breck, D. W., Eversole, W. G., Milton, R. M., Reed, T. B., & Thomas, T. L. (1956). Crystalline zeolites. I. The properties of a new synthetic zeolite, type A. *Journal of the American Chemical Society*, *78*(23), 5963–5971. https://doi.org/10.1021/ja01604a001

Chandrasekhar, S. (1996). Influence of metakaolinization temperature on the formation of zeolite 4A from kaolin. *Clay Minerals*, *31*(2), 253–261. https://doi.org/10.1180/claymin.1996.031.2.11

Chen, H. L., Li, X. Y., Rooke, J. C., Zhang, Y. H., Yang, X. Y., Tang, Y., Xiao, FS., & Su, B. L. (2012). Hierarchically structured zeolites: Synthesis, mass transport properties and applications. *Journal of Materials Chemistry*, *22*(34), 17381–17403. https://doi.org/10.1039/C2JM31958C

El Bojaddayni, I., Küçük, M. E., El Ouardi, Y., Issam, J., El Barkany, S., Moradi, K., Repo, E., Laatikainen, K., & Ouammou, A. (2023). A review on synthesis of zeolites from natural clay resources and waste ash: Recent approaches and progress. *Minerals Engineering*, *198*, Article 108086. https://doi.org/10.1016/j.mineng.2023.108086

Eluwa, V. C., Obasa, P. A., Gana, E. M., & Igbonekwu, C. A. (2024). Synthesis and characterization of zeolite A from Aloji kaolin via hydrothermal method. *Journal of Materials Science Research and Reviews*, *7*(4), 592–601. https://doi.org/10.9734/jmsrr/2024/v7i4352

Filho, S. H. S., Bieseki, L., Silva, A. R., Maia, A. A. B., San Gil, R. A. S., & Pergher, S. B. C. (2015). Synthesis of Zeolite A employing Amazon kaolin waste. *Cerâmica*, *61*(360), 409–413. https://doi.org/10.1590/0366-69132015613601898

Gleichmann, K., Unger, B., & Brandt, A. (2016). Industrial zeolite molecular sieves. In *Zeolites - Useful Minerals* (Chapter 5). IntechOpen. https://doi.org/10.5772/63442

Gougazeh, M., & Buhl, J. Ch. (2014). Synthesis and characterization of zeolite A by hydrothermal transformation of natural Jordanian kaolin. *Journal of the Association of Arab Universities for Basic and Applied Sciences*, *15*(1), 35–42. https://doi.org/10.1016/j.jaubas.2013.03.007

Hart, A., Wood, J., & Al-Qureshi, H. (2025). Methodological review of zeolite synthesis from industrial waste and natural clays, and the fabrication. *Materials*, *9*, Article 101113. https://doi.org/10.1016/j.nxmate.2025.101113

Hartati, P., Purwanto, A., & Widodo, E. (2020). A review on the synthesis of kaolin-based zeolite and the effect of impurities. *Journal of the Chinese Chemical Society*, *68*(1), 1–26. https://doi.org/10.1002/jccs.202000185

Kırdeciler, S. K., & Akata, B. (2020). One-pot fusion route for the synthesis of zeolite 4A using kaolin. *Advanced Powder Technology*, *31*(10), 4336–4343. https://doi.org/10.1016/j.apt.2020.09.012

Kovo, A. S., Holmes, S. M., Rios, C. A., Otaru, A. J., Abdulkareem, A. S., & Eluwa, V. C. (2025). Synthesis of zeolites from different kaolin deposits worldwide. *Applied Clay Science*, *269*(1), Article 107757. https://doi.org/10.1016/j.clay.2025.107757

Król, M., & Rożek, P. (2018). The effect of calcination temperature on metakaolin structure for the synthesis of zeolites. *Clay Minerals*, *53*(4), 657–663. https://doi.org/10.1180/clm.2018.49

Lim, W. R., Lee, Ch. H., & Hamm, S. Y. (2021). Synthesis and characteristics of Na-A zeolite from natural kaolin in Korea. *Materials Chemistry and Physics*, *261*, Article 124230. https://doi.org/10.1016/j.matchemphys.2021.124230

Liu, X. D., Wang, Y. P., Cui, X. M., He, Y., & Mao, J. (2013). Influence of synthesis parameters on NaA zeolite crystals. *Powder Technology*, *243*, 184–193. https://doi.org/10.1016/j.powtec.2013.03.048

Lowell, S., Shields, J. E., Thomas, M. A., & Thommes, M. (2004). *Characterization of Porous Solids and Powders: Surface Area, Pore Size and Density*. Springer Science & Business Media. https://doi.org/10.1007/978-1-4020-2303-3

Maia, A. Á. B., Neves, R. F., Angélica, R. S., Herbert, H., Straub, C., & Saalwächter, K. (2014). Use of Si and Al MAS NMR to study thermal activation of kaolinites from Brazilian Amazon kaolin wastes. *Applied Clay Science*, *87*, 189–196. https://doi.org/10.1016/j.clay.2013.10.028

Maia, A. Á. B., Neves, R. F., Angélica, R. S., & Herbert, H. (2015). Synthesis, optimisation and characterisation of the zeolite NaA using kaolin waste from the Amazon Region. Production of Zeolites KA, MgA and CaA. *Applied Clay Science*, *108*, 55–60. https://doi.org/10.1016/j.clay.2015.02.017

Mejía de Gutiérrez, R., Torres, J., Vizcayno, C., & Castello, R. (2008). Influence of the calcination temperature of kaolin on the mechanical properties of mortars and concretes containing metakaolin. *Clay Minerals*, *43*(2), 177–183. https://doi.org/10.1180/claymin.2008.043.2.02

Moore, D. M., & Reynolds Jr., R. C. (1997). *X-ray Diffraction and the Identification and Analysis of Clay Minerals* (2nd ed.). Oxford University Press.

Nakano, T., & Nozue, Y. (2007). Orbital degeneracy and magnetic properties of potassium clusters incorporated into nanoporous crystals of zeolite A. *Journal of Computational Methods in Sciences and Engineering*, *7*(5-6), 443–462. https://doi.org/10.3233/JCM-2007-75-610

Nurhidayati, Hasfianti, F. E., & Wahyudi, K. (2020). Kajian teknoekonomi kaolin Belitung sebagai bahan substitusi impor pada produksi fiber cement board. *Jurnal Keramik dan Gelas Indonesia*, *29*(2), 152–164. https://doi.org/10.32537/jkgi.v29i2.6565

Paranuk, A., Saavedra Huayta, J.A., & Khrisonidi, V. (2018). Separation of binary solutions on the basis of zeolites. In R. M. Nageeb & P. N. Palanisamy (Eds.), *Zeolites and Their Applications* (Vol. 73513). IntechOpen. https://doi.org/10.5772/intechopen.73513

Pasabeyoglu, P., Moumin, G., de Oliveira, L., Roeb, M., & Akata, B. (2023). Solarization of the zeolite production: Calcination of kaolin as proof-of-concept. *Journal of Cleaner Production*, *414*, Article 137611. https://doi.org/10.1016/j.jclepro.2023.137611

Pérez-Botella, E., Valencia, S., & Rey, F. (2022). Zeolites in adsorption processes: State of the art and future prospects. *Chemical Reviews*, *122*(24), 17647–17695. https://doi.org/10.1021/acs.chemrev.2c000140

Ramírez, A. M., García, A. J. T., Camacho, B. R., Badillo, C. M. L., Mojica, J. I. M., & Martínez-Gómez, C. M. (2021). Simple synthesis of hierarchically structured X zeolite from geothermal nanosilica and its evaluation in the dehydration of aqueous solutions of ethanol. *Chemical Papers*, *75*(1), 337–349. https://doi.org/10.1007/s11696-020-01302-2

Rocha, J., Klinowski, J., & Adams, J. M. (1991). Synthesis of zeolite Na-A from metakaolinite revisited. *Journal of the Chemical Society,*

*Faraday Transactions*, *87*(18), 3091–3097. https://doi.org/10.1039/FT9918703091

Sachse, A., Grau-Atienza, A., Jardim, E. O., Linares, N., Thommes, M., & García-Martínez, J. (2017). Development of intracrystalline mesoporosity in zeolites through surfactant-templating. *Crystal Growth & Design*, *17*(8), 4289–4305. https://doi.org/10.1021/acs.cgd.7b00619

Sazali, N., & Harun, Z. (2022). One-shot of the hydrothermal route for synthesis of zeolite LTA using kaolin. *Journal of Inorganic and Organometallic Polymers and Materials*, *32*(9), 3508–3520. https://doi.org/10.1007/s10904-022-02364-5

Shukla, P., Dong, K., Rudolph, V., Bhatia, S. K., Bajaj, H. C., & Jasra, R. V. (2019). Adsorptive dehydration of ethanol using 3A zeolite: An evaluation of transport behaviour in a two-phase zeolite pellet. *Adsorption*, *25*(8), 1611–1623. https://doi.org/10.1007/s10450-019-00145-y

Simo, M., Sivashanmugam, S., Brown, C. J., & Hlavacek, V. (2009). Adsorption/desorption of water and ethanol on 3A zeolite in near-adiabatic fixed bed. *Industrial & Engineering Chemistry Research*, *48*(20), 9247–9260. https://doi.org/10.1021/ie900446v

Sinchangreed, A., Watcharamaisakul, S., & Janphuang, P. (2025). Preparation and characterization of zeolite A synthesized from Narathiwat white clay. *Bulletin of Chemical Reaction Engineering & Catalysis*, *20*(3), 553–559. https://doi.org/10.9767/bcrec.20.3.11122.553-559

SNOWPEAK. (2026). *Molecular Sieve 3A*. Henan Snowpeak Molecular Sieve Co., Ltd. https://www.snowpeakzeolite.com/product-item/molecular-sieve-3a/

Tahraoui, Z., Nouali, H., Marichal, C., Forler, P., Klein, J., & Daou, T. J. (2020). Influence of the compensating cation nature on the water adsorption properties of zeolites. *Molecules*, *25*(4), Article 944. https://doi.org/10.3390/molecules25040944

Thommes, M., Kaneko, K., Neimark, A. V., Olivier, J. P., Rodriguez-Reinoso, F., Rouquerol, J., & Sing, K. S. W. (2015). Physisorption of gases, with special reference to the evaluation of surface area and pore size distribution (IUPAC Technical Report). *Pure and Applied Chemistry*, *87*(9-10), 1051–1069. https://doi.org/10.1515/pac-2014-1117

Treacy, M. M. J., & Higgins, J. B. (2001). *Collection of Simulated XRD Powder Patterns for Zeolites* (4th rev. ed.). Elsevier.

Ulfah, M., Praputri, E., Firdaus, & Muchtiar, Y. (2023). Synthesis and characterization of a zeolite pellet using natural kaolinite clays from Indonesia as binder and their application in dehydration ethanol. *AIP Conference Proceedings*, *2691*(1), Article 050002. https://doi.org/10.1063/5.0115184

Verboekend, D., Nuttens, N., Locus, R., Van Aelst, J., Verolme, P., Groen, J. C., Pérez-Ramírez, J., & Sels, B. F. (2016). Synthesis, characterisation, and catalytic evaluation of hierarchical faujasite zeolites: Milestones, challenges, and future directions. *Chemical Society Reviews*, *45*(12), 3331–3352. https://doi.org/10.1039/C5CS00520E

Yao, G., Lei, J., Zhang, X., Sun, Z., & Zheng, S. (2018). One-step hydrothermal synthesis of zeolite X powder from natural low-grade diatomite. *Materials*, *11*(6), Article 906. https://doi.org/10.3390/ma11060906

Yin, H., Liu, H., Bu, Y., Chen, W., Ding, F., Lin, W., & Zhang, Y. (2024). Regulation of reactivity of calcined ultrafine kaolin products. *Processes*, *12*(10), Article 2268. https://doi.org/10.3390/pr12102268

Zhou, Z., Jin, G., Liu, H., Wu, J., & Mei, J. (2014). Crystallization mechanism of zeolite A from coal kaolin using a two-step method. *Applied Clay Science*, *97–98*, 110–114. https://doi.org/10.1016/j.clay.2014.05.015

© 2026. The Author(s). This article is an open access article distributed under the terms and conditions of the Creative Commons Attribution-ShareAlike 4.0 (CC BY-SA) International License (http://creativecommons.org/licenses/by-sa/4.0/)